Biosensors and Bioelectronics 216 (2022) 114638

Contents lists available at ScienceDirect

Biosensors and Bioelectronics

journal homepage: www.elsevier.com/locate/bios

A graphene nanoplatelet-polydopamine molecularly imprinted biosensor for Ultratrace creatinine detection

Yixuan Li [a], Liuxiong Luo [b], Mengyan Nie [a], Andrew Davenport [c], Ying Li [d], Bing Li [a,*], Kwang-Leong Choy [a,**]

[a] Institute for Materials Discovery, Department of Chemistry, Faculty of Mathematical & Physical Sciences, University College London, London, WC1E 7JE, UK
[b] School of Materials Science and Engineering, Central South University, Changsha, 410083, PR China
[c] UCL Department of Renal Medicine, Royal Free Hospital, University College London, Rowland Hill Street, London, NW3 2PF, UK
[d] Dept of Brain Repair and Rehabilitation, UCL Institute of Neurology, Queen Square, London, WC1N 3BG, UK

ARTICLE INFO

Keywords:
Ultratrace creatinine detection
Molecularly imprinted polymer
Electrochemical biosensor
Graphene nanoplatelet
Polydopamine
Kidney disease

ABSTRACT

Accurate and reliable analysis of creatinine is clinically important for the early detection and monitoring of patients with kidney disease. We report a novel graphene nanoplatelet (GNP)/polydopamine (PDA)-molecularly imprinted polymer (MIP) biosensor for the ultra-trace detection of creatinine in a range of body fluids. Dopamine hydrochloride (DA) monomers were polymerized using a simple one-pot method to form a thin PDA-MIP layer on the surface of GNP with high density of creatinine recognition sites. This novel surface-MIP strategy resulted in a record low limit-of-detection (LOD) of 2×10^{-2} pg/ml with a wide dynamic detection range between 1×10^{-1}-1×10^{9} pg/ml. The practical application of this GNP/PDA-MIP biosensor has been tested by measuring creatinine in human serum, urine, and peritoneal dialysis (PD) fluids. The average recovery rate was 93.7–109.2% with relative standard deviation (RSD) below 4.1% compared to measurements made using standard clinical laboratory methods. Our GNP/PDA-MIP biosensor holds high promise for further development as a rapid, accurate, point-of-care diagnostic platform for detecting and monitoring patients with kidney disease.

1. Introduction

Creatinine, the product of creatine and phosphocreatine metabolism, is produced by non-enzymatic reactions of phosphocreatine in muscle. The excretion of creatinine in the urine depends primarily upon the filtration rate of the glomeruli, and urinary creatinine clearance is used in clinical practice as an assessment of kidney function (Broza et al., 2019; Hill et al., 2016; Liu et al., 2018). As such, it is important to develop accurate methods for measuring creatinine in body fluids to detect and monitor patients with kidney disease.

The physiological concentrations of serum and urinary creatinine in healthy humans range between 35 and 140 μM and 71–265 μmol d^{-1} kg^{-1}, respectively (Kalantar-Zadeh et al., 2021). The most used method for creatinine detection in clinical practice is based on the Jaffe colorimetric method (Chen et al., 2019), using picric acid to react with creatinine and form orange-red complexes, which can then be detected and measured. However, this colorimetric assay is potentially susceptible to interference by pigmented compounds, including bilirubin and some medications (Wen et al., 2014). Several other methods have also been developed for measuring creatinine, including enzymatic catalysis (Hewavitharana and Bruce, 2003) and noble metal nanoparticles (NPs)-based detection (Mohabbati-Kalejahi et al., 2012). Detection with the enzyme creatinase shows excellent sensitivity, but the stability of the assay is restricted due to the limited active time of enzyme. As for biosensors based on noble metal NPs, such as AuNPs (Du et al., 2016) and AgNPs (Viswanath et al., 2017), the expensive raw materials and inadequate selectivity prevent their development for clinical use. Thus, a stable and ultrasensitive assay is urgently needed for accurate and reliable creatinine measurement in clinical body fluids.

Molecularly imprinted polymer (MIP) biosensors have been developed over recent times for the ultrasensitive detection of small molecules (Uygun et al., 2015). These biosensors simulate the interaction between antibodies and antigens in nature, allowing the monomers to "capture" template molecules during the polymerization process and form three-dimensional imprinting sites that can then specifically recognize target molecules (Bagheri et al., 2018; El-Beshlawy et al.,

* Corresponding author.
** Corresponding author.
E-mail addresses: bing.li@ucl.ac.uk (B. Li), k.choy@ucl.ac.uk (K.-L. Choy).

https://doi.org/10.1016/j.bios.2022.114638
Received 18 July 2022; Received in revised form 27 July 2022; Accepted 11 August 2022
Available online 18 August 2022

2021; Li et al., 2013). A few MIP-based biosensors have been previously developed for the detection of creatinine. For example, the MIP-Au-SPE/PVC-COOH (Diouf et al., 2017) has reported to have an LOD of 0.16 ng/ml whilst maintaining high selectivity. Others, such as MIP/Sol-Gel/Graphite modified electrode (Patel et al., 2010) and Fe_3O_4/PANI-MIES/MGCE (Wen et al., 2014) were reported to have the sensitivity at 0.064 mA μmol^{-1} and 0.173 mA μmol^{-1}, respectively. However, these MIP biosensors have several disadvantages, including the cumbersome polymerization process, poor conductivity of polymer which leads to the insufficient sensitivity, and deeply embedded template molecules, which result in a high background signal and a narrower detection range (Yan and Row, 2006).

In this paper, a surface-MIP biosensor fabricated with molecularly imprinted PDA coating on GNP was proposed. The novel surface-MIP technology could avoid an overly-thick MIP layer, and so allow more template molecules to locate on, or close to the polymer surface during the polymerization process. This ensures that template molecules can be removed more thoroughly, so leading to a wider detection range. GNP is a cost-effective and highly conductive nano-carbon material with a large surface-to-volume ratio (Geim, 2009; Li et al., 2015). Given the conductive network formed by GNP which enables fast electron transfer, a GNP-based biosensor could potentially have an excellent sensitivity and an extremely low LOD. DA monomers can self-polymerize and also adhere to other substrates under suitable conditions, which means that the GNP/PDA-MIP composite can be synthesized through an simple one-pot method, so avoiding the complicated preparation processes of conventional MIPs.

We report on the application of a GNP/PDA-MIP biosensor for the detection of creatinine in various body fluids, This biosensor was observed to have a record LOD at femtomolar level, along with excellent sensitivity, selectivity, and accuracy over a wide detection range. Due to these characteristics, this GNP/PDA-MIP biosensor offers the potential for the detection of creatinine in other body fluids, so providing a promising non-invasive point of care (POC) testing for creatinine, to readily detect and monitor patients with kidney disease.

2. Experimental section

2.1. Materials and instruments

All reagents including creatinine, graphene nanoplatelets, dopamine hydrochloride, ammonium persulfate (AP), HNO_3 (ACS reagent, 70%), HCl (ACS reagent, 37%), H_2SO_4, glycine, glucose, urea, uric acid, creatine, sarcosine, bilirubin, ascorbic acid, lactic acid (85%, FCC), cholesterol, KCl, $K_3Fe(CN)_6$, $K_4Fe(CN)_6{\cdot}3H_2O$, $Na_2HPO_4{\cdot}12H_2O$, KH_2PO_4 were purchased from Sigma-Aldrich, Gillingham, UK. All chemicals, unless specified, were of analytical reagent grade.

Prepared materials were characterized using Raman spectroscopy (Renishaw inVia, Stockport, UK), Fourier transform infrared spectroscopy (FT-IR, Spectrum Two, PerkinElmer, Beaconsfield, UK), X-ray diffraction (XRD, X'Pert 3 MRD, Malvern, UK, CuKα radiation, Leeds, UK), Scanning Electron Microscopy (SEM, Hitachi 8230, Maidenhead, UK), Transmission electron microscope (TEM, FEI Talos F200X, ThermoFisher Scientific, Hemel Hempstead, UK)) and Thermogravimetric Analysis (TGA, Perkin-Elmer 4000, Beaconsfield, UK).

Electrochemical measurements were conducted using a Gamry 1010 workstation Gamry, Warminster, USA). A modified glassy carbon electrode (GCE, 3 mm in diameter) was used as the working electrode. Pt and Ag/AgCl (3 M KCl) were used as counter and reference electrode, respectively. All potentials in the text were with respect to the Ag/AgCl reference electrode.

2.2. Preparation of GNP/PDA-MIP composite

The preparation principle of GNP/PDA-MIP is shown in Fig. 1. DA monomers formed a PDA film by polymerization after attaching to the

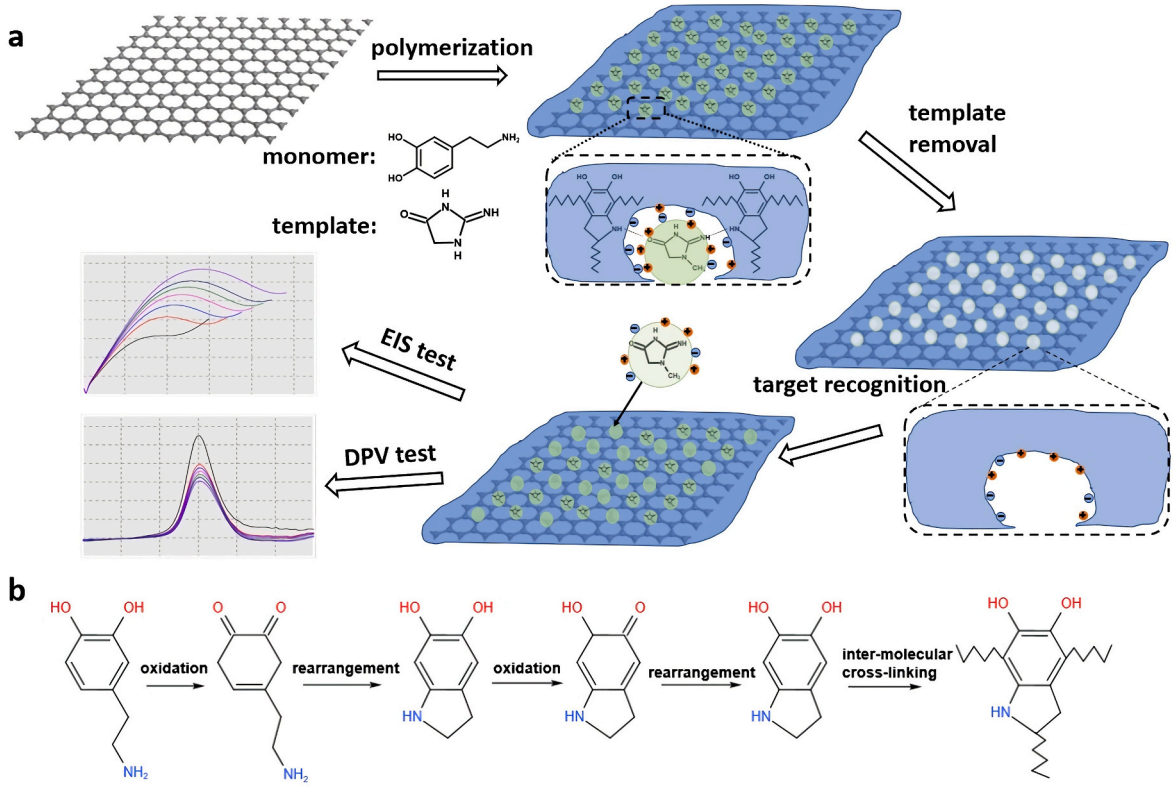

Fig. 1. Schematic representation for the preparation of GNP/PDA-MIP. (a) The fabrication and application process of GNP/PDA-MIP. (b) The formation mechanism of DA spontaneous oxidative polymerization.

GNP surface (Yin et al., 2018). Creatinine molds were implanted into the PDA membranes based on intermolecular forces in suitable micropores. Subsequently, by vigorous stirring in elution to remove the embedded creatinine template molecules, the GNP/PDA-MIP composite with creatinine recognition ability could be obtained. The GNP/PDA-MIP modified electrode generated using the self-assembly process through drop-casting (Yin et al., 2018).

The specific preparation process was as follows: 0.174 g $Na_2HPO_4{\cdot}12H_2O$ and 0.012 g KH_2PO_4 were dissolved in 60 ml deionized water to prepare phosphate buffered saline (PBS). After thorough stirring, the solution was evenly divided into two portions, each of 30 ml. One ml of acid-treated GNP (10 mg/ml) was dispersed in 30 ml of PBS buffer and magnetically stirred. The preparation process and characterization of GNP acid treatment are shown in Figs. S1 and S2, respectively. 40.58 mg DA and 33.17 mg creatinine (m_{Cre}:m_{DA} = 4.5:5.5) were added to another 30 ml PBS buffer solution and sonicated for 1 h under ice bath condition until completely dissolved. 23.95 mg of AP (n_{AP}:n_{DA} = 1:2) was added to the mixed solution, and the mixture then stirred uniformly for 24 h at room temperature. Finally, the product was washed successively with water and 1 M HCl by centrifugation to remove unreacted reactants until no template molecule could be detected in the washing solution by spectrophotometry.

2.3. Electrochemical measurements

Electrochemical measurements were performed using 150 mL of 0.01 M PBS solution (pH = 7.4) containing 1 mM $K_3Fe(CN)_6$/$K_4Fe(CN)_6$ and 0.1 M KCl. The electrochemical behavior and performance of the GNP/PDA-MIP modified electrodes were characterized by cyclic voltammetry (CV), differential pulse voltammetry (DPV), and electrochemical impedance spectroscopy (EIS). CV was performed at a scan rate of 100 mV/s over a potential range between −0.8 V and +0.8 V. DPV was performed at a scan rate of 50 mV/s over a potential range between −0.5 V and +1.0 V. EIS measurements were conducted under the open circuit voltage, with a frequency range of 0.1 Hz–100 kHz and a signal amplitude of 5 mV. The electrochemical behavior and performance of the GNP/PDA-non-MIP (NIP) modified electrodes were also evaluated using the same setup. NIP refers to the composite prepared using the same method as MIP without template molecules added. The electrochemical active surface area (ECSA) test was further performed through CV to compare GNP/PDA-MIP and GNP/PDA-NIP composite and shown in SI (Fig. S3).

3. Results and discussion

3.1. Characterization of GNP/PDA-MIP composite

To demonstrate the successful encapsulation of PDA on the acid-

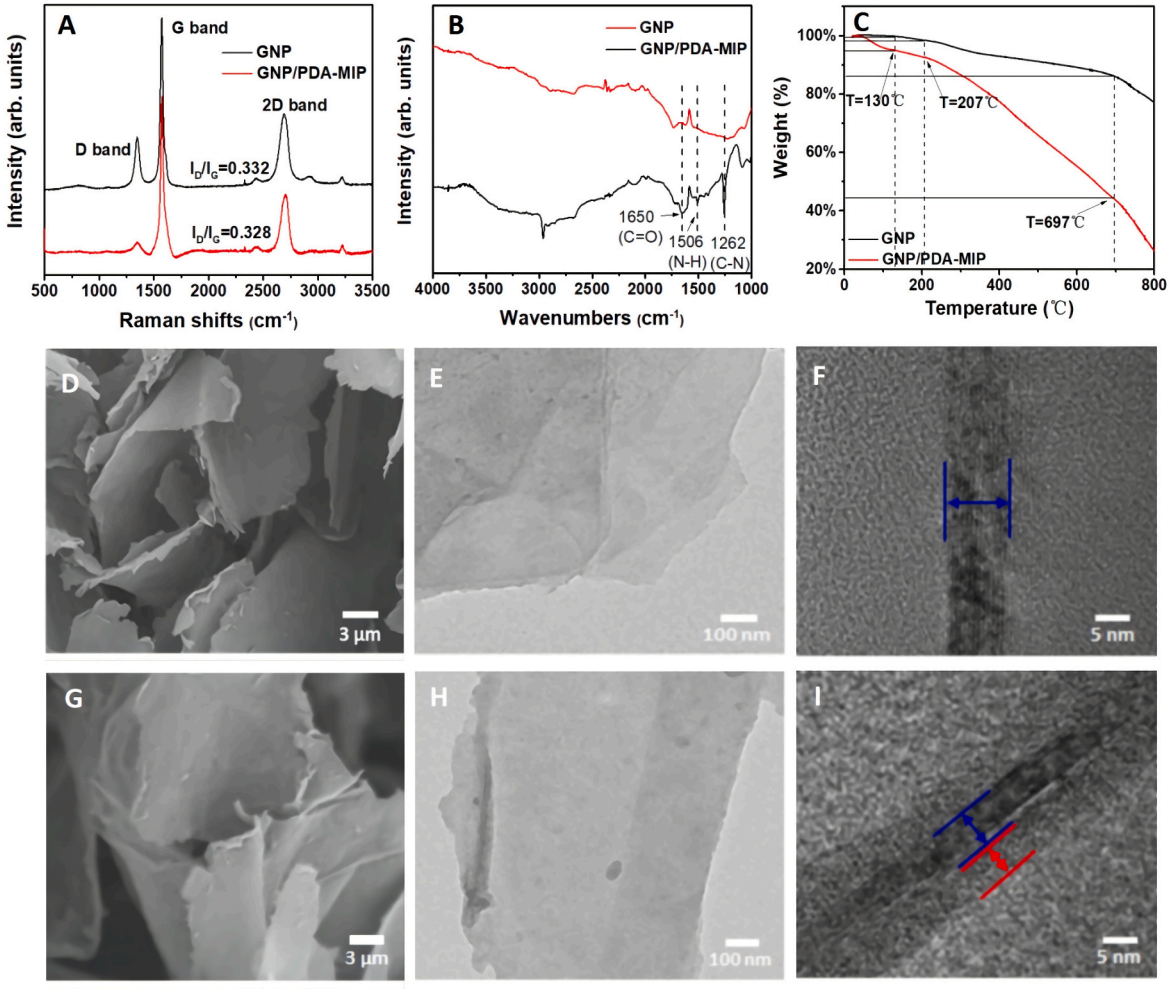

Fig. 2. Characterization of the GNP/PDA-MIP composite. (A) Raman spectra of GNP and GNP/PDA-MIP; (B) FT-IR spectrum of GNP and GNP/PDA-MIP; (C) TGA plot of GNP and GNP/PDA-MIP; SEM images of (D) GNP, (G) GNP/PDA-MIP; TEM images of (E) GNP, (H) GNP/PDA-MIP; HRTEM images of (F) GNP, (I) GNP/PDA-MIP (The striped area indicated by blue lines represents GNP, and the surrounding area indicated by red lines represents PDA).

treated GNP, Raman, FT-IR, and TGA characterization were conducted on the material. Raman spectra analysis (Fig. 2(A)), shows that the GNP-based material has two distinct bands D (attributed to defective *sp3*-hybridized carbon atoms) and G (reflecting the E_{2g} vibration of *sp2*-hybridized graphitized carbon atoms) at 1344 cm^{-1} and 1570 cm^{-1} respectively with an I_D/I_G ratio of 0.332. After PDA coating, the I_D/I_G ratio decreased to 0.328, which is due to the partial removal of the oxygen-containing functional groups between the graphite layers during the polymerization process of the DA monomers (Alkhouzaam et al., 2021; Li et al., 2019; Mahdi et al., 2022).

Comparison of the FT-IR spectra of GNP/PDA-MIP and acid-treated GNP, (Fig. 2(B)), demonstrates that several characteristic peaks appeared after PDA coating. The characteristic peaks at 1262 cm^{-1}, 1506 cm^{-1} and 1650 cm^{-1} are attributed to the C–N bond, N–H bond, and C═O groups respectively, which all attribute to the amide group in PDA (Ha et al., 2021). Fig. 2(C) shows the TGA curves of acid-treated GNP and GNP/PDA-MIP from 20 to 800 °C. The final weight loss of acid-treated GNP was about 21.8 wt% due to the decomposition of labile oxygen and the pyrolysis of ring carbons. On the other hand, the pyrolysis of GNP/PDA-MIP has four steps. Initially due to a loss of water vapour, then as the temperature increases pyrolysis of oxygen-containing functional groups (-COOH, –COH, and –C═O, etc.) began. The pyrolysis rate began to accelerate above 207 °C, mainly due to the start of PDA pyrolysis. Above 697 °C, the ring carbons also began to pyrolyze, with a weight loss of 72.8 wt% at 800 °C. Compared to the weight loss experienced by acid-treated GNP, the amount of PDA grafted to the GNP surface was circa 51 wt% (Alkhouzaam et al., 2021).

We compared the morphology between GNP and GNP/PDA-MIP by SEM and TEM. The size of acid-treated GNP was circa 20 μm in diameter, with an observable smooth surface and multilayer structure (Fig. 2(D)). Whereas after PDA encapsulation (Fig. 2(G)), the surface became rough with a blurred appearance due to the charging effect on the non-conductive PDA (Yin et al., 2018). Besides, compared to the TEM image of acid-treated GNP (Fig. 2(E)), few particles appeared on the surface of the product after PDA coating (Fig. 2(H)) due to self-polymerization of a small amount of non-adhered DA monomers into microspheres (Du et al., 2016; Yousefi et al., 2016). The high-resolution TEM (HRTEM) images Fig. 2(F) and (I) clearly showed that the thickness of the GNP was about 4–7 nm, whereas the prepared MIP composite formed a thin PDA shell on the surface of GNP with a thickness circa 4.9 nm, demonstrating that the surface of GNP had been successfully coated with PDA thin film. The morphology contrast between GNP/PDA-MIP and GNP/PDA-NIP was shown in Fig. S4.

3.2. Optimization of GNP/PDA-MIP composite

A series of experiments were performed to optimize the GNP/PDA-MIP composite, including exploring the effect of mass ratio between template molecules and monomers, amount of oxidant, polymerization time, and adsorption time to target molecules on the performance of the composite. The mass ratio of template molecules to monomers affects the number of imprinted cavities in the MIP framework, which in turn affects the recombination and recognition capabilities of the biosensors. The fewer imprinted cavities will result in the smaller change of resistance of charge transfer (ΔRct) during tests (Liu et al., 2017). As shown in Fig. S5(A), the ΔRct changed markedly with the change in mass ratio of creatinine/DA. The ΔRct reached a maximum when the mass ratio of creatinine/DA was 4.5:5.5. An inadequate amount of monomers leads to fewer imprinting cavities, whereas excessive monomers results in an increased amount of cross-linking, so that a significant amount of the templates will be deeply embedded and unremovable, thus reducing detection efficiency (Sun et al., 2016).

Usually, the pH values of human urine and serum are around 5–8 and 7.35–7.45, respectively. Therefore, in order to simulate the body fluid environment, the preparation of GNP/PDA-MIP composite was carried out in PBS buffer at pH 7.4. Since DA monomers can only self-polymerize at pH 8.5, an oxidant AP was required to promote the polymerization of DA monomers (Wei et al., 2010), and its optimal ratio to DA monomers was explored, as shown in Fig. S5(B). The amount of DA monomers was fixed as 40.58 mg, the maximum EIS response was obtained with 23.95 mg of AP, a ratio of oxidant to DA monomers at 1:2 for the complete polymerization to form imprinted polymer with sufficient imprinting cavities.

The duration of monomers polymerization determines the thickness of the polymer layer. The highest EIS response was obtained after stirring for 24 h (Fig. S5(C)). Shorter stirring times resulted in the insufficient polymerization of DA monomers, forming an incomplete MIP layer with fewer recognition sites. However, a longer polymerization period leads to over cross-linked monomers, resulting in more unreachable encapsulated imprinted cavities in the polymer layer for the target molecules. Insufficient binding sites therefore resulted in less combined creatinine when the material was under adsorption test, further resulting in the lower ΔRct (Yin et al., 2018).

Fig. S5(D) shows the effect of different incubation time on the EIS response to creatinine detection at 1 μg/ml. The ΔRct value increased linearly with the incubation time and then saturated around 10 min. This indicates that the creatinine molecules could quickly bind to the imprinting sites on the MIP surface in the first 10 min, and thereafter adsorption and desorption of creatinine in the polymer film reached a dynamic equilibrium (Liu et al., 2017).

3.3. Electrochemical behavior of GNP/PDA-MIP modified electrodes

CV has been used to characterize the electrochemical behavior of the modified electrode (Yousefi et al., 2021). Fig. 3(A) shows the typical CV curves of GNP/PDA-MIP modified electrode in $K_3Fe(CN)_6/K_4Fe(CN)_6$ electrolyte. The peak current decreases significantly when the electrode surface is covered with GNP/PDA-MIP layer, so preventing $[Fe(CN)_6]^{3-/4-}$ from reaching the electrode surface for redox reactions. The peak redox current of the CV curve increased after the template molecules were removed, indicating that the removal of template molecules caused the reduced impedance of GNP/PDA-MIP composite, which further led to the increased redox current. When 1 μg/ml creatinine was added to the solution to bind with GNP/PDA-MIP, a decrease in peak current was observed. This was because the original imprinted cavities on the MIP layer became occupied by the creatinine again, thus reducing the electron transfer of redox probes.

As a comparison, CV curves of GNP/PDA-NIP are also shown in Fig. 3 (B). After coating the electrode surface with GNP/PDA-NIP, the redox current decreases, which is similar to the GNP/PDA-MIP modified electrode. However, after elution, the curves show no significant differences, and similarly the redox current remained unchanged after incubation with creatinine. These affects are due to the absence of active imprinted cavities on the GNP/PDA-NIP layer, indicating that GNP/PDA-NIP cannot recognize the target creatinine molecules.

EIS test was used to further characterize the electrochemical behavior of the GNP/PDA-MIP modified electrode, as shown in Fig. 3 (C). When the GNP/PDA-MIP composite was coated on the electrode, the curve-a with a Rct value of 135 Ω changed to curve-b which does not show an obvious semicircle that can be used to calculate Rct. Then, after the removal of template molecules, it changed to curve-c with Rct value of 1945 Ω, and then increased to 3649 Ω (curve-d) after the electrode was incubated with 1 μg/ml creatinine. The semicircular part at the high frequency region corresponds to the charge transfer process, while the linear part at the low frequency region represents the diffusion control process in the EIS curve. The value of Rct is mainly affected by the charge-transfer impedance. During the MIP preparation, functional monomers are concentrated around the isolated templates, leaving the continuous dielectric space to separate the imprinting sites. After the template molecules are removed, the cavities with surrounding charges emerge. Thus, each imprinted cavity resembles a molecular capacitor that is fully charged in advance. Template cavity recombination occurs

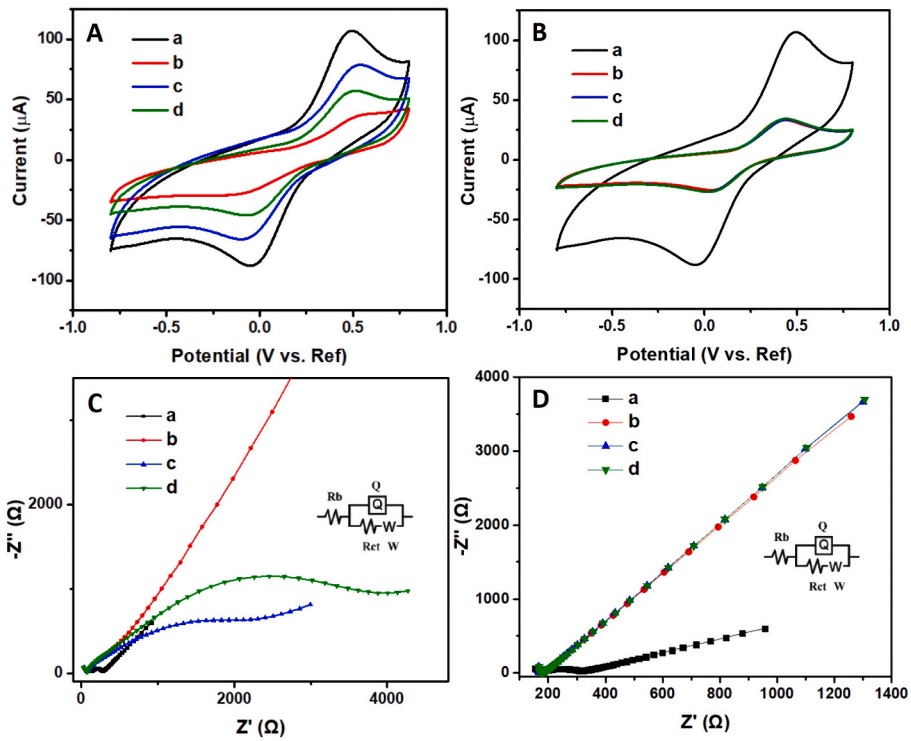

Fig. 3. Electrochemical behavior of the GNP/PDA-MIP modified electrode. (A) Cyclic voltammograms of the bare electrode (curve-a), GNP/PDA-MIP modified electrode before (curve-b) and after washing with elution (curve-c), GNP/PDA-MIP modified electrode after rebinding with creatinine (1 μg/ml) (curve-d). (B) Cyclic voltammograms of the bare electrode (curve-a), GNP/PDA-NIP modified electrode before (curve-b) and after washing with elution (curve-c), GNP/PDA-NIP modified electrode after rebinding of creatinine (1 μg/ml) (curve-d). (C) Nyquist plot of the bare electrode (curve-a), GNP/PDA-MIP modified electrode before (curve-b) and after washing with elution (curve-c), GNP/PDA-MIP modifed electrode after rebinding of creatinine (1 μg/ml) (curve-d). (D) Nyquist plot of the bare electrode (curve-a), GNP/PDA-NIP modified electrode before (curve-b) and after washing with elution (curve-c), GNP/PDA-NIP modified electrode after rebinding of creatinine (1 μg/ml) (curve-d).

as creatinine recognition or detection proceeds. At this point a one-to-one response should be achieved between charged groups from the creatinine surface and the cavity wall. The different charges create a series of "ion pair" analogs that neutralize each other. For cavity capacitors, this appears to be a "discharge" process. Therefore, as creatinine molecules are eluted and recombined (curve c and d), these molecular capacitors continuously undergo a reversible "charge-discharge" process, which leads to the changes of the Rct (Yang et al., 2019). As for MIP without template molecules desorption (curve-b), the structure is similar to NIP but without imprinting vacancies. The diffusion control process dominates the impedance so becoming more like a conductor in the high frequency region with linear signals (Reddy and Gobi, 2013). The test result of GNP/PDA-NIP shown in Fig. 3(D) further supports this theory. NIP without recognition sites only present linear signals without change in Nyquist plot during the creatinine desorption or resorption, as it is only controlled by mass transfer.

The EIS results further verify that the GNP/PDA-MIP modified electrode has an excellent ability to identify target molecules, which is consistent with the CV detection results (Liu et al., 2017).

3.4. Determination of sensitivity and LOD

GNP/PDA-MIP modified electrodes were used to detect creatinine at different concentrations. Fig. 4(A) demonstrates that as the creatinine concentration increases, the semicircle radius (Rct value) in the impedance curve also increases, indicating that the material is sensitive to creatinine concentration. The calibration plot of Fig. 4(B) shows that ΔRct increases linearly with the logarithmic concentration of creatinine in the range of 1×10^{-1}-1×10^{9} pg/ml, with a correlation coefficient of 0.9860. The calibration plot was evaluated by three times determination, and the RSD value of each concentration was below 5.71%. The LOD was determined to be 2×10^{-2} pg/ml (S/N = 3) (Liu et al., 2017).

DPV was also used to test the performance of GNP/PDA-MIP modified electrode. Fig. 4(C) shows that with increasing creatinine concentration the peak DPV current decreases, as the current is primarily generated by the redox of $Fe(CN)_6^{3-/4-}$ on the electrode surface (Diouf et al., 2017). As the amount of creatinine adsorbed by the GNP/PDA-MIP increases, more imprinting sites are occupied, so reducing the electron transfer of the redox probes. The calibration plot of Fig. 4(D) demonstrates that in the range of 1×10^{-1}-1×10^{9} pg/ml, the current value decreases linearly with the logarithmic concentration of creatinine with a correlation coefficient of 0.9988. The calibration plot was evaluated by three times determination with a RSD value less than 1.01% and LOD at 3×10^{-2} pg/ml (S/N = 3).

Tests for GNP/PDA-NIP modified electrodes were also performed to act as a comparison. It can be seen from Fig. 4(E) and (F) that GNP/PDA-NIP shows no responses when creatinine concentrations are changed with either EIS or DPV testing. These results further confirm the ultrasensitive response of our GNP/PDA-MIP modified electrode to creatinine.

3.5. Determination of other key biosensing performance

In order to characterize the selectivity of our GNP/PDA-MIP modified electrode for creatinine, some potentially interfering compounds from human body fluids (glycine, sarcosin, urea, glucose, uric acid, bilirubin, creatine, cholesterol, lactic acid, ascorbic acid) were added to the same EIS detection solution as controls (Reddy and Gobi, 2013; Wen et al., 2014). Fig. 5(A) indicates that the value of ΔRct detected by GNP/PDA-MIP biosensors for creatinine was much higher than those for other interfering molecules. The maximum value of ΔRct was only 6.3% of creatinine detection signals, which indicates that GNP/PDA-MIP has excellent specificity for the recognition of creatinine.

GNP/PDA-MIP was immobilized on an electrode and reused four times. As shown in Fig. 5(B), the value of EIS response kept 97.5% after three reuses, which demonstrates excellent reusability of the electrode. With the fourth use, the value of ΔRct decreased to 70.6%, compared to the first use. This was due to partial detachment or destruction of the MIP material upon repeated elution of creatinine molecules. As for the reproducibility of producing the modified electrode, five separate batches of GNP/PDA-MIP modified electrodes were compared, with a RSD value of 4.85%, confirming the excellent reproducibility of electrode fabrication (Fig. 5(C)). The initial response of the GNP/PDA-MIP coated electrode remained at 94.8% after four months storage at room

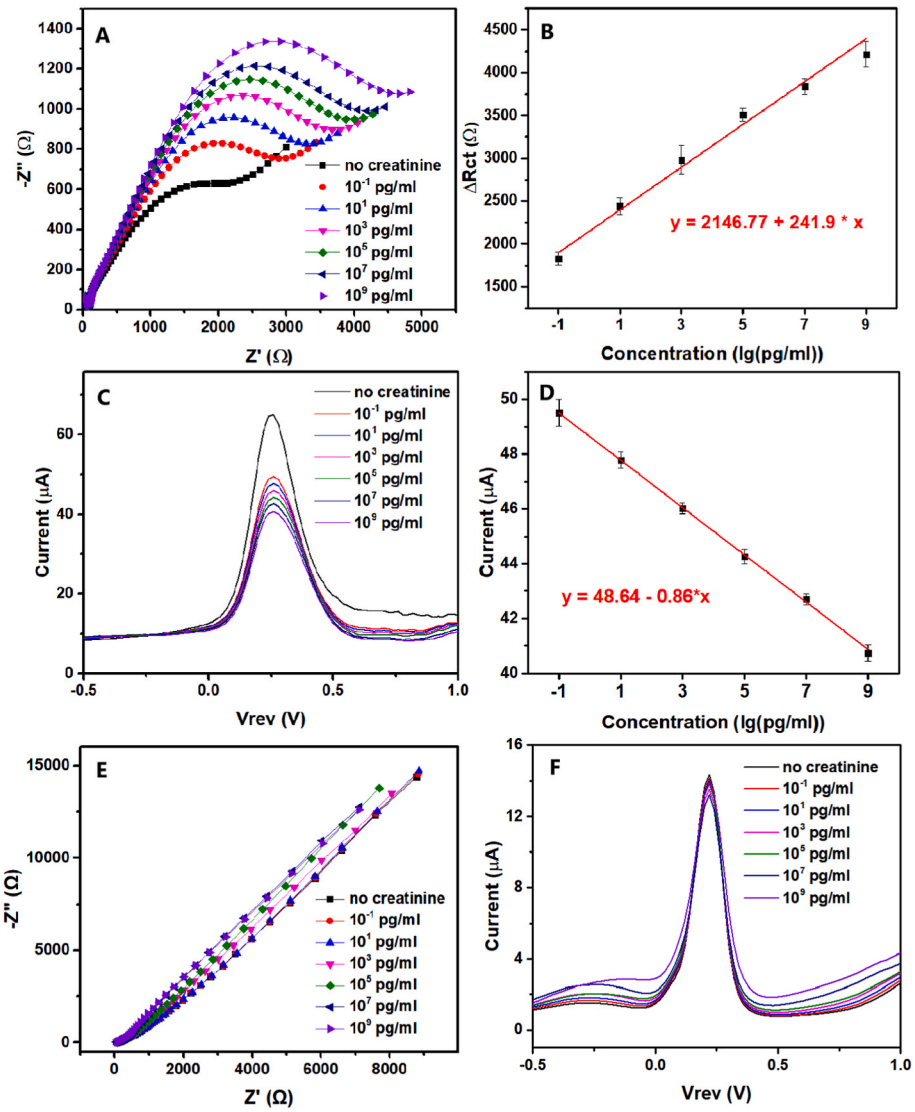

Fig. 4. Determination of GNP/PDA-MIP and GNP/PDA-NIP modified electrodes in different concentrations of creatinine solution. (A) The EIS response of the GNP/PDA-MIP modified electrode towards different concentration of creatinine in electrolyte. (B) The calibration plot of ΔRct versus the log concentration of creatinine. (C) The DPV response of the GNP/PDA-MIP modified electrode towards different concentration of creatinine in electrolyte. (D) The calibration plot of the current values versus the log concentration of creatinine. (E) The EIS response of the GNP/PDA-NIP modified electrode towards different concentration of creatinine in electrolyte. (F) The DPV response of the GNP/PDA-NIP modified electrode towards different concentration of creatinine in electrolyte.

temperature, with the RSD value of 3.31% (Fig. 5(D)) (Wen et al., 2014), indicating good long-term stability.

3.6. Creatinine detection in clinical samples

National research ethics permission was obtained to obtain serum, urine, and peritoneal dialysis (PD) fluid samples from anonymous and unidentifiable patients with renal disease (19/LO/1031). Patients provided written informed consent in keeping with the Helsinki accord. To reduce the matrix effect and the effects of liquid viscosity, the creatinine concentration was measured using spike-and-recovery assessment by three times determination, which is the standard technique in clinical settings. All samples were diluted a thousand times in PBS buffer. As shown in Table 1, the average recovery was 93.7–109.2% with RSD below 4.1% for replicate samples. The high recovery rates of creatinine concentrations in clinically relevant samples suggest that this biosensor is promising for POC testing in the clinical setting.

4. Conclusions

In conclusion, we report a novel MIP electrochemical, biosensor for the ultrasensitive detection of creatinine using GNP/PDA composites. A layer of PDA was coated onto the surface of GNP through a simple and environmental-friendly one-pot method. Our studies exemplified by the measurement of creatinine demonstrate the high selectivity, excellent sensitivity and reliable stability of this technique mainly due to the high conductivity of GNP and the abundant imprinted cites of the surface-MIP. The most prominent advantages of this GNP/PDA-MIP biosensor are the extremely wide linear response range and record low LOD compared to current creatinine biosensors (Table S1). This strategy not only provides a POC detection method for the frontline clinical diagnosis of creatinine content, but also offers the potential for POC detection of many other biomarkers in body fluids for the diagnosis of a variety of diseases.

CRediT authorship contribution statement

Yixuan Li: Conceptualization, Data curation, Methodology, Writing - original draft. **Liuxiong Luo:** Data curation. **Mengyan Nie:** Methodology. **Andrew Davenport:** Supervision, Writing - review & editing. **Ying Li:** Supervision. **Bing Li:** Supervision, Funding acquisition, Writing - original draft, Writing - review & editing. **Kwang-Leong Choy:** Conceptualization, Funding acquisition, Supervision.

Declaration of competing interest

The authors declare that they have no known competing financial interests or personal relationships that could have appeared to influence

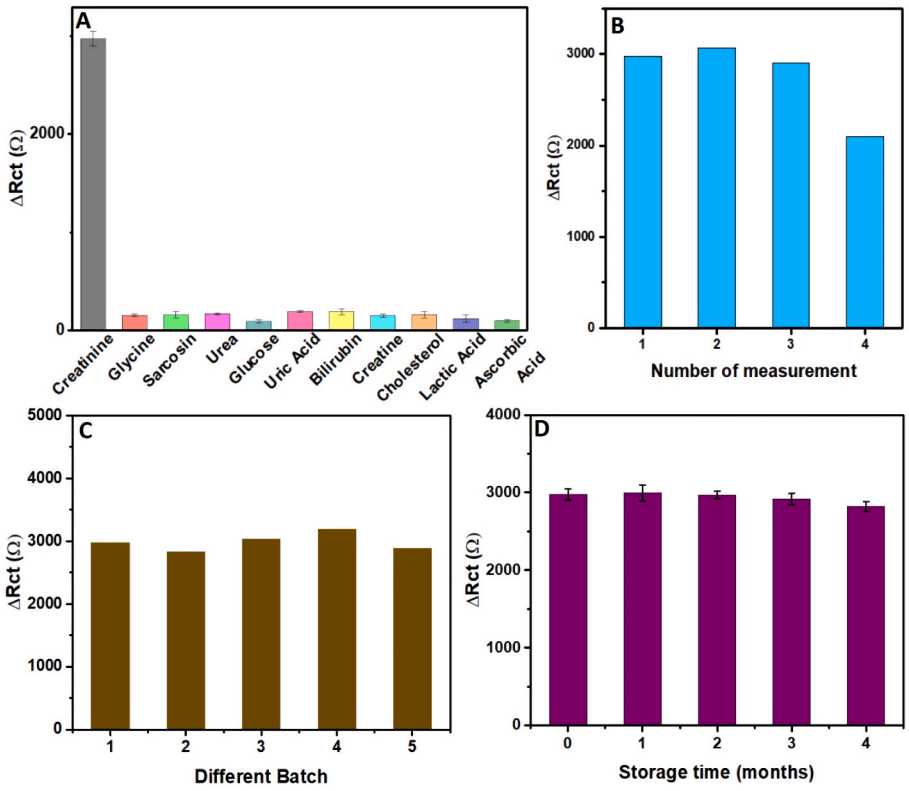

Fig. 5. Several performance tests through EIS detection. (A) The value of ΔRct to the presence of creatinine and other interferents individually at 10 μmol/L. (B) The value of ΔRct to the presence of creatinine at 10 μmol/L in several measurements. (C) The value of ΔRct to the presence of creatinine at 10 μmol/L in five batches of GNP/PDA-MIP. (D) The value of ΔRct to the presence of creatinine at 10 μmol/L in four months.

Table 1
Determination of creatinine in clinical samples (n = 3).

Sample	Found (μM)[a]	Spiked (μM)[b]	Detected (μM)[c]	Recovery (%)[d]	RSD (%)
		1	2.13	99.6	2.7
serum	1.14	2	3.04	96.7	3.8
		3	4.23	102.3	4.1
		2	4.82	93.7	1.5
urine	3.14	3	6.11	99.5	2.3
		4	5.26	105.8	2.2
		0.5	1.40	95.4	3.6
PD fluid	0.97	1.5	2.51	101.6	0.9
		2.5	3.79	109.2	1.8

[a] The value of creatinine concentration of diluted clinical samples tested by UK nationally accredited hospital chemical pathology laboratory using standard methods.
[b] The value of known amount of creatinine aqueous solution.
[c] The clinical body fluid sample was added into the known amount of creatinine aqueous solution and the response was measured.
[d] The ratio of detected value/(found value + spiked value).

the work reported in this paper.

Data availability

Data will be made available on request.

Acknowledgements

The authors thank the Edmond J Safra Foundation, Alzheimer's Research Trust (Grant No. ARUK-PPG2021B-001), China Scholarship Council (CSC) and the University College London (UCL).

Appendix A. Supplementary data

Supplementary data to this article can be found online at https://doi.org/10.1016/j.bios.2022.114638.

References

Alkhouzaam, A., Qiblawey, H., Khraisheh, M., 2021. Membranes 11 (2), 86.
Bagheri, N., Khataee, A., Habibi, B., Hassanzadeh, J., 2018. Talanta 179, 710–718.
Broza, Y.Y., Zhou, X., Yuan, M., Qu, D., Zheng, Y., Vishinkin, R., Khatib, M., Wu, W., Haick, H., 2019. Chem. Rev. 119 (22), 11761–11817.
Chen, T.K., Knicely, D.H., Grams, M.E., 2019. JAMA 322 (13), 1294.
Diouf, A., Motia, S., El Hassani, N.E.A., El Bari, N., Bouchikhi, B., 2017. IEEE, pp. 1–3.
Du, H., Chen, R., Du, J., Fan, J., Peng, X., 2016. Ind. Eng. Chem. Res. 55 (48), 12334–12340.
El-Beshlawy, M.M., Abdel-Haleem, F.M., Barhoum, A., 2021. Electroanalysis 33 (5), 1244–1254.
Geim, A.K., 2009. science 324 (5934), 1530–1534.
Ha, Y.-M., Kim, Y.N., Jung, Y.C., 2021. Polymers 13 (8), 1274.
Hewavitharana, A., Bruce, H., 2003. J. Chromatogr., B 784 (2), 275–281.
Hill, N.R., Fatoba, S.T., Oke, J.L., Hirst, J.A., O'Callaghan, C.A., Lasserson, D.S., Hobbs, F.R., 2016. PLoS One 11 (7), e0158765.
Kalantar-Zadeh, K., Jafar, T.H., Nitsch, D., Neuen, B.L., Perkovic, V., 2021. Lancet 379 (9811), 165–180.
Li, B., Pan, G., Avent, N.D., Lowry, R.B., Madgett, T.E., Waines, P.L., 2015. Biosens. Bioelectron. 72, 313–319.
Li, C., Li, X., Sun, X., Zhang, X., Duan, L., Yang, X., Wang, L., Lü, W., 2019. Nanoscale Res. Lett. 14 (1), 1–9.
Li, X., Zhang, L., Wei, X., Li, J., 2013. Electroanalysis 25 (5), 1286–1293.
Liu, S., Ma, Y., Cui, M., Luo, X., 2018. Sens. Actuator B-Chem. 255, 2568–2574.
Liu, W., Ma, Y., Sun, G., Wang, S., Deng, J., Wei, H., 2017. Biosens. Bioelectron. 92, 305–312.
Mahdi, M.A., Yousefi, S.R., Jasim, L.S., Salavati-Niasari, M.J.I.J.o.H.E., 2022 47(31), 14319-14330..
Mohabbati-Kalejahi, E., Azimirad, V., Bahrami, M., Ganbari, A., 2012. Talanta 97, 1–8.
Patel, A.K., Sharma, P.S., Prasad, B.B., 2010. Thin Solid Films 518 (10), 2847–2853.
Reddy, K.K., Gobi, K.V., 2013. Sens. Actuator B-Chem. 183, 356–363.
Sun, Y., Du, H., Lan, Y., Wang, W., Liang, Y., Feng, C., Yang, M., 2016. Biosens. Bioelectron. 77, 894–900.
Uygun, Z.O., Uygun, H.D.E., Ermiş, N., Canbay, E., 2015. Biosensors - Micro and Nanoscale Applications, pp. 85–108.

Viswanath, K.B., Devasenathipathy, R., Wang, S.F., Vasantha, V., 2017. Electroanalysis 29 (2), 559–565.
Wei, Q., Zhang, F., Li, J., Li, B., Zhao, C., 2010. Polym. Chem. 1 (9), 1430–1433.
Wen, T., Zhu, W., Xue, C., Wu, J., Han, Q., Wang, X., Zhou, X., Jiang, H., 2014. Biosens. Bioelectron. 56, 180–185.
Yan, H., Row, K.H., 2006. Int. J. Mol. Sci. 7 (5), 155–178.
Yang, C., Ji, X.-F., Cao, W.-Q., Wang, J., Zhang, Q., Zhong, T.-L., Wang, Y., 2019. Sens. Actuator B-Chem. 282, 818–823.
Yin, Z.-Z., Cheng, S.-W., Xu, L.-B., Liu, H.-Y., Huang, K., Li, L., Zhai, Y.-Y., Zeng, Y.-B., Liu, H.-Q., Shao, Y., 2018. Biosens. Bioelectron. 100, 565–570.
Yousefi, S., Ghanbari, D., Salavati, N.M., 2016..
Yousefi, S.R., Alshamsi, H.A., Amiri, O., Salavati-Niasari, M.J.J.o.M.L., 2021 337, 116405..